arXiv:1304.7030v1 [nucl-th] 25 Apr 2013

Photon elliptic flow in relativistic heavy-ion collisions: hadronic versus partonic sources

O. Linnyk,* V.P. Konchakovski, and W. Cassing
Institute for Theoretical Physics, Justus Liebig University of Giessen, 35392 Giessen, Germany

E. L. Bratkovskaya
Institute for Theoretical Physics, Johann Wolfgang Goethe University, 60438 Frankfurt am Main, Germany; Frankfurt Institute for Advanced Studies, 60438 Frankfurt am Main, Germany;
(Dated: April 29, 2013)

We study the transverse momentum spectrum and the elliptic flow v_2 of photons produced in Au+Au collisions at $\sqrt{s_{NN}} = 200$ GeV using the Parton-Hadron-String Dynamics (PHSD) transport approach. As sources for photon production, we incorporate the interactions of off-shell quarks and gluons in the strongly interacting quark-gluon plasma (sQGP) ($q+\bar{q} \to g+\gamma$ and $q(\bar{q})+g \to q(\bar{q})+\gamma$), the decays of hadrons ($\pi \to \gamma+\gamma$, $\eta \to \gamma+\gamma$, $\omega \to \pi+\gamma$, $\eta' \to \rho+\gamma$, $\phi \to \eta+\gamma$, $a_1 \to \pi+\gamma$) as well as their interactions ($\pi+\pi \to \rho+\gamma$, $\rho+\pi \to \pi+\gamma$). The PHSD calculations reproduce the transverse momentum spectrum, the effective temperature T_{eff} and the elliptic flow v_2 of direct photons as measured by the PHENIX Collaboration. The photons produced in the QGP contribute about 50% to the observed spectrum, but have small v_2. We find that the large direct photon v_2 – comparable to that of hadrons – is attributed to the intermediate hadronic scattering channels and hadronic resonance decays not subtracted from the data. The QGP phase causes the strong elliptic flow of photons indirectly, by enhancing the v_2 of final hadrons due to the partonic interaction in terms of explicit parton collisions and the mean-field potentials. On the other hand, the presence of the QGP radiation is manifest in the slope of the direct photon spectrum, leading to T_{eff} far above the critical temperature for the deconfinement phase transition.

PACS numbers: 25.75.-q, 13.85.Qk, 24.85.+p

I. INTRODUCTION

The electromagnetic emissivity of strongly interacting matter at finite temperature and baryonic chemical potential is a subject of longstanding interest and is explored in particular in relativistic nucleus-nucleus collisions, where the photons (and dileptons) measured experimentally provide a time-integrated picture of the collision dynamics. This 'camera' also records the early stages of such collisions due to the low final state interactions of electromagnetic signals [1], but the 'picture' is blurred by the emission at later stages. Fortunately, the 'final picture' of the hot and dense matter created early in the collision in part can be restored by independently measuring hadronic channels and subtracting the associated light signals. The corrected spectra then are denoted as 'direct photons'.

The recent observation by the PHENIX Collaboration [2] that the elliptic flow $v_2(p_T)$ of 'direct photons' produced in minimal bias Au+Au collisions at $\sqrt{s_{NN}} = 200$ GeV is comparable to that of the produced pions was a surprise and in contrast to the theoretical expectations and predictions [3–6]. Indeed, the photons produced by partonic interactions in the quark-gluon plasma phase have not been expected to show considerable flow because - in a hydrodynamical picture - they are dominated by the emission at high temperatures, i.e. in the initial phase before the elliptic flow fully develops. On the other hand, the dominant hadronic sources of photon production – decays of π and η mesons – have been subtracted by the PHENIX Collaboration from the total photon spectrum using a model-independent method [2] and therefore do not explain the observed strong momentum anisotropy of the direct photons. This has lead also to the suggestion that the photon v_2 observed might be a signature for more unconventional sources such as the pre-equilibrium gluon interaction with the magnetic field [7, 8], enhanced emission of photons at the QGP surface [9] or novel assumptions for the transverse parton acceleration in the QGP [10, 11].

In the present study we apply the Parton-Hadron-String Dynamics (PHSD) transport approach to investigate the photon production in Au+Au collisions at $\sqrt{s_{NN}} = 200$ GeV. In the past the PHSD approach has provided a consistent description of the bulk properties of heavy-ion collisions – rapidity spectra, transverse mass distributions, azimuthal asymmetries of various particle species – from low Super-Proton-Synchrotron (SPS) to top Relativistic-Heavy-Ion-Collider (RHIC) energies [12] and was successfully used also for the analysis of dilepton production from hadronic and partonic sources at SPS, RHIC and Large-Hadron-Collider (LHC) energies [13–15]. In the hadronic sector, PHSD is equivalent to the Hadron-String Dynamics (HSD) approach [16–18], in which the photon production at lower SPS energies has been investigated in Ref. [19] with an emphasis on the role of meson-meson interactions. In the present study we extend the approach to higher collision energies by explicitly incorporating photon production in the strongly interacting quark-gluon plasma (sQGP). Indeed, the deconfined state of matter was found to be created in heavy-ion collisions at RHIC [20–23] for a couple of fm/c [24] leaving substantial traces especially in the dilepton yield above invariant masses of 1.2 GeV [13–15].

---

*Electronic address: Olena.Linnyk@theo.physik.uni-giessen.de

The photon radiation from the partonic phase is consequently expected to show a large contribution to the transverse momentum spectrum of produced photons [3–6, 25–35], the slope of which was even used to deduce an 'average temperature' of the QGP [36, 37] which we address as an 'apparent inverse slope parameter' or energy scale for the photonic radiation. The transition to the strongly interacting QGP in the initial phase of the heavy-ion collisions and the subsequent hadronization is treated dynamically in the PHSD approach. It is therefore of interest to calculate the photon production in relativistic heavy-ion collisions from hadronic and partonic interactions consistently within the PHSD transport approach, in which the microscopic and non-equilibrium evolution of the nucleus-nucleus collision is independently controlled by a multitude of other hadronic and electromagnetic observables in a wide energy range [13–15, 24, 38, 39].

II. PHOTON PRODUCTION SOURCES WITHIN THE PHSD TRANSPORT APPROACH

The PHSD model [24, 39] is an off-shell transport approach that consistently describes the full evolution of a relativistic heavy-ion collision from the initial hard scatterings and string formation through the dynamical deconfinement phase transition to the quark-gluon plasma as well as hadronization and to the subsequent interactions in the hadronic phase. In PHSD the transition from the partonic to hadronic degrees of freedom is described by covariant transition rates for the fusion of quark-antiquark pairs to mesonic resonances or three quarks (antiquarks) to baryonic states, i.e., by the dynamical hadronization [40]. The two-particle correlations resulting from the finite width of the parton spectral functions are taken into account dynamically in the PHSD by means of the *generalized* off-shell transport equations [41] that go beyond the mean field or Boltzmann approximation [42, 43]. The transport theoretical description of quarks and gluons in the PHSD is based on the Dynamical Quasi-Particle Model (DQPM) for partons that is constructed to reproduce lattice QCD (lQCD) results for a quark-gluon plasma in thermodynamic equilibrium. The DQPM provides the mean-fields for gluons/quarks and their effective 2-body interactions that are implemented in the PHSD. For details about the DQPM model and the off-shell transport approach we refer the reader to the review in Ref. [42].

A. Hadronic sources of photon production

As sources of photon production - on top of the general dynamical evolution - we consider hadronic [32] as well as partonic [25, 26] interactions. Let us first describe the hadronic contributions, which consist of the photon production from hadronic decays and the interactions of final as well as intermediate mesons produced throughout the evolution of the nucleus-nucleus collision:

1) Photon production by mesonic decays $(\pi^0, \eta, \eta', \omega, \phi, a_1)$, where the mesons are produced first in baryon-baryon (BB), meson-baryon (mB) or meson-meson (mm) collisions. The photon production from the mesonic decays represents a 'background' for the search of the direct photons, however, this background can only partly be subtracted from the signal by data driven methods. Just as in the earlier work within the HSD model [19], we consider the contributions from the photon decay of the following mesons:

$$\begin{aligned}
&\pi^0 \to \gamma + \gamma, \\
&\eta \to \gamma + \gamma, \\
&\eta' \to \rho + \gamma, \\
&\omega \to \pi^0 + \gamma, \\
&\phi \to \eta + \gamma, \\
&a_1 \to \pi + \gamma.
\end{aligned}$$

The decay probability is calculated according to the corresponding branching ratios taken from the latest compilation by the Particle Data Group [44], updating slightly the values applied in earlier HSD investigations at SPS energies [19]. The broad resonances – including the a_1, ρ, ω mesons – in the initial or final state are treated in PHSD in line with their (in-medium) spectral functions, as implemented and explained in detail in Ref. [19].

2) Additionally to the resonance/meson decay channels, the photons can be produced in mesonic collisions. We consider the direct photon production in the scattering processes

$$\begin{aligned}
\pi\pi &\to \rho\gamma, \\
\pi\rho &\to \pi\gamma,
\end{aligned}$$

accounting for all possible charge combinations.

We calculate the cross sections for the processes $\pi\pi \to \rho\gamma, \pi\rho \to \pi\gamma$ as in Ref. [19], i.e. the total cross section $\sigma_{\pi\pi\to\rho\gamma}(s, \rho_N)$ is obtained by folding the vacuum cross section $\sigma^0_{\pi\pi\to\rho\gamma}(s, M)$ with the (in-medium) spectral function of the ρ meson:

$$\sigma_{\pi\pi\to\rho\gamma}(s, \rho_N) = \int\limits_{M_{min}}^{M_{max}} dM\ \sigma^0_{\pi\pi\to\rho\gamma}(s, M)\ A(M, \rho_N)\ P(s). \tag{1}$$

Here $A(M, \rho_N)$ denotes the meson spectral function for given total width Γ^*_V:

$$A_V(M,\rho_N) = C_1 \, \frac{2}{\pi} \, \frac{M^2 \, \Gamma^*_V(M,\rho_N)}{(M^2 - M_0^{*2}(\rho_N))^2 + (M\Gamma^*_V(M,\rho_N))^2}, \tag{2}$$

with the normalization condition for any ρ_N, $\int_{M_{min}}^{M_{lim}} A_V(M,\rho_N)\ dM = 1$, where $M_{lim} = 2$ GeV is chosen as an upper limit for the numerical integration while the lower limit of the vacuum ρ spectral function corresponds to the 2π decay $M_{min} = 2m_\pi$. M_0^* is the pole mass of the vector meson spectral function which is $M_0^*(\rho_N = 0) = M_0$ in vacuum, however, might be shifted in the medium (e.g. for the dropping mass scenario). Furthermore, the vector meson width is the sum of the vacuum total decay width and collisional width:

$$\Gamma^*_V(M,\rho_N) = \Gamma_V(M) + \Gamma_{coll}(M,\rho_N). \tag{3}$$

In Eq. (1) the function $P(S)$ accounts for the fraction of the available part of the full spectral function $A(M,\rho_N)$ at given energy $\sqrt{s}$, integrated over the mass M up to $M_{max} = \sqrt{s}$, with respect to the total phase space.

The cross section $\sigma^0_{\pi\pi\to\rho\gamma}(s,M)$ is taken from the model by Kapusta et al. [27] with the ρ-meson mass considered as a dynamical variable, i.e $m_\rho \to M$:

$$\begin{aligned} \frac{d\sigma}{dt}\left(\pi^\pm\pi^0 \to \rho^\pm\gamma\right) \ &= \\ -\frac{\alpha g_\rho^2}{16 s p_{CM}^2} \Bigg[\frac{(s-2M^2)(t-m_\pi^2)^2}{M^2(s-M^2)^2} &+ \frac{m_\pi^2}{M^2} - \frac{9}{2} \\ + \frac{(s-6M^2)(t-m_\pi^2)}{M^2(s-M^2)} &+ \frac{4(M^2-4m_\pi^2)s}{(s-M^2)^2} \\ + \frac{4(M^2-4m_\pi^2)}{t-m_\pi^2} &\left(\frac{s}{s-M^2} + \frac{m_\pi^2}{t-m_\pi^2}\right)\Bigg]. \end{aligned} \tag{4}$$

The photon production in the $\pi+\rho$ interaction is calculated analogously (cf. Ref. [19] for details).

In particular the photon production in secondary meson interactions is sensitive to the properties of the ρ meson in the medium [19, 45, 46]. In this respect, we stress here that the yields and the in-medium spectral functions of vector mesons in PHSD have been independently constrained by the comparison to the data on dilepton mass-spectra (see Refs. [13, 14, 38]).

B. Partonic sources of photon production

We continue with the description of photon production in the interactions of quarks and gluons in the quark-gluon plasma, which dominantly proceeds through the quark annihilation and the gluon Compton scattering processes:

$$\begin{aligned} q + \bar{q} \ &\to \ g + \gamma \\ q(\bar{q}) + g \ &\to \ q(\bar{q}) + \gamma. \end{aligned}$$

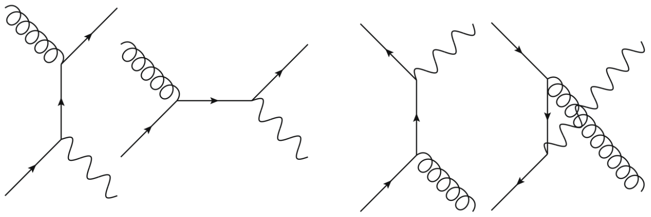

FIG. 1: (Color on-line) Feynman diagrams for the partonic sources ($q(\bar{q}) + g \to q(\bar{q}) + \gamma$ and $q + \bar{q} \to g + \gamma$) included in the PHSD calculations.

The diagrams contributing to these scattering processes at tree level are presented in Fig. 1.

In the strongly interacting QGP, the gluon and quark propagators (in PHSD) differ significantly from the non-interacting propagators such that bare production amplitudes can no longer be used. The off-shell quarks and gluons have finite masses and widths, which parametrize the resummed interaction of the QGP constituents. The perturbative QCD results for the cross sections of the processes in Fig. 1 have to be generalized in order to include the finite masses for fermions and gluons as well as their broad spectral functions. In Refs. [47], the influence of the gluon off-shellness (fixed to $m_g^2 = |\vec{k_g}|^2$) on the photon production was studied but the quark masses had been neglected and the spectral functions were assumed to be δ-functions (quasi-particle approximation). On the other hand, in Ref. [48] a finite quark mass was incorporated in the elementary cross sections for both the quark annihilation and the gluon-Compton scattering processes, but the gluon was taken to be massless and the quasiparticle approximation remained. The resulting cross sections of Ref. [48] are instructive and still compact enough to be explicitly shown here for illustration of the quark mass effect:

$$\begin{aligned} \frac{d\sigma}{dt}(q\bar{q} \to \gamma g) \ &= \\ -\frac{4}{9}\left(\frac{e_q^2}{e^2}\right)^2 \frac{8\pi\alpha_S \ \alpha_{EM}}{s(s-4m_q^2)} &\left[\left(\frac{m_q^2}{t-m_q^2} + \frac{m_q^2}{u-m_q^2}\right)^2 \right. \\ + \left(\frac{m_q^2}{t-m_q^2} + \frac{m_q^2}{u-m_q^2}\right) &\left. - \frac{1}{4}\left(\frac{t-m_q^2}{u-m_q^2} + \frac{u-m_q^2}{t-m_q^2}\right)\right] \end{aligned} \tag{5}$$

$$\begin{aligned} \frac{d\sigma}{dt}(gq \to \gamma q) \ &= \\ \frac{1}{6}\left(\frac{e_q^2}{e^2}\right)^2 \frac{8\pi\alpha_S \ \alpha_{EM}}{(s-m_q^2)^2} &\left[\left(\frac{m_q^2}{s-m_q^2} + \frac{m_q^2}{u-m_q^2}\right)^2 \right. \\ + \left(\frac{m_q^2}{s-m_q^2} + \frac{m_q^2}{u-m_q^2}\right) &\left. - \frac{1}{4}\left(\frac{s-m_q^2}{u-m_q^2} + \frac{u-m_q^2}{s-m_q^2}\right)\right] \end{aligned} \tag{6}$$

It is obvious from equations (5) and (6) that the quark off-shellness leads to higher twist corrections ($\sim$

$m_q^2/s, m_q^2/t, m_q^2/u)$. These corrections are small in hard hadron scattering at high center-of-mass energy $\sqrt{s} > 10$ GeV, but become substantial for photon production in the sQGP, where the characteristic $\sqrt{s}$ of parton collisions is of the order of a few GeV.

As mentioned above, the formulae (5) and (6) have to be further generalized in order to be included into the PHSD transport approach, in particular, by incorporating the finite mass for the gluon and departing from the quasiparticle approximation. Note also that in (5) and (6) the masses of quarks and antiquarks were assumed equal, which is not the case for the broad strongly-interacting particles in the PHSD. For this purpose, we use the relation between the real photon production cross section and the cross section for dilepton production [36]:

$$\frac{d\sigma(\gamma)}{dt} = \lim_{M\to 0} \frac{3\pi}{\alpha} \frac{M^2}{L(M)} \frac{d^2\sigma(e^+e^-)}{dM^2 dt}, \tag{7}$$

where M^2 is the invariant mass squared of the lepton pair, i.e. the virtuality of the virtual photon, and the kinematical factor $L(M)$ is given by

$$L(M) = \sqrt{1 - \frac{4m_e^2}{M^2}}(1 + \frac{2m_e^2}{M^2}), \tag{8}$$

with m_e denoting the lepton mass. The evaluation of cross sections for dilepton production by off-shell partons, taking into account finite masses for quarks, antiquarks (with generally $m_q \neq m_{\bar{q}}$) and gluons m_g as well as their finite spectral width (by integrating over the mass distributions in analogy with the equation (1)) has been carried out in Refs. [49, 50] We refer the reader to the work [50] for details of the calculations, where the phenomenological parametrizations from the DQPM for the quark and gluon propagators and their interaction strength were used. Since the resulting formulae are quite lengthy, we do not repeat them here.

We take $d^2\sigma(e^+e^-)/dM^2dt$ from Ref. [50] and used the relation (7) to implement the real photon production in the off-shell quark and gluon interactions into the PHSD transport approach. In each interaction of $q+\bar{q}$ or $q/\bar{q}+g$, the photon production probability and the elliptic flow of the produced photon are recorded differentially in transverse momentum p_T and rapidity y.

III. RESULTS

A. Spectra

The results for the inclusive photon spectrum as a sum of all the considered partonic as well as hadronic sources for the photons produced in minimal bias Au+Au collisions at $\sqrt{s_{NN}} = 200$ GeV is presented in Fig. 2 as a function of the transverse momentum p_T at mid-rapidity $|y| < 0.35$. The leading contributions are the decays of the π^0 and η mesons. Since these 'late' hadronic sources are less sensitive to the creation of the hot and dense medium and to its properties, they are subtracted experimentally to access the 'direct' photon spectrum.

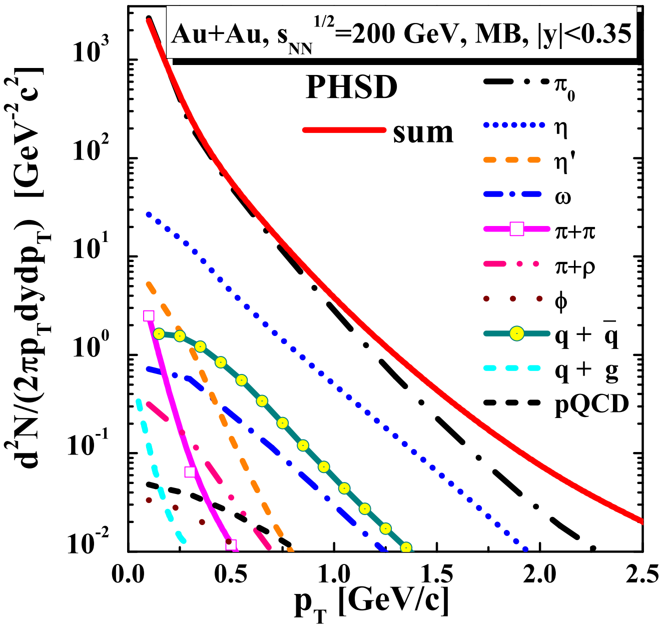

FIG. 2: (Color on-line) Photon transverse momentum (p_T) spectra from PHSD for minimal bias Au+Au collisions at $\sqrt{s_{NN}} = 200$ GeV (full solid upper line) at mid-rapidity $|y| < 0.35$. The channel decomposition of the inclusive photon spectrum is given in the legend.

The experimental data on the remaining 'direct' photon spectrum are compared to the PHSD calculations (without π^0 and η decays) in Fig. 3. The measured transverse momentum spectrum dN/dp_T is reproduced, if the partonic and the remaining hadronic sources are summed up (upper solid line). We find that the radiation from the sQGP constitutes about half of the observed number of photons. The radiation from hadrons and their interaction – which are not measured separately so far – give a considerable contribution, too, especially at low transverse momentum. On the other hand, we explicitly show in the bottom panel of Fig. 3 that the purely hadron/string scenario as incorporated within the HSD transport approach (dashed line) does not explain the data.

The spectrum presented in Fig. 3 may be approximated by an exponential spectrum of p_T below 2 GeV to extract an 'effective temperature' as was done by the PHENIX Collaboration in Ref. [36, 37]. The extracted 'effective temperature' is obviously reproduced by the theoretical calculations within PHSD, see Table I. In the theoretical approach, we have the possibility to separate the yields according to the production sources and therefore to extract the 'effective temperatures' of the photons stemming from parton interactions and those of hadronic origin (see Table I). One observes that the characteristic temperature scale for the photons produced in the QGP

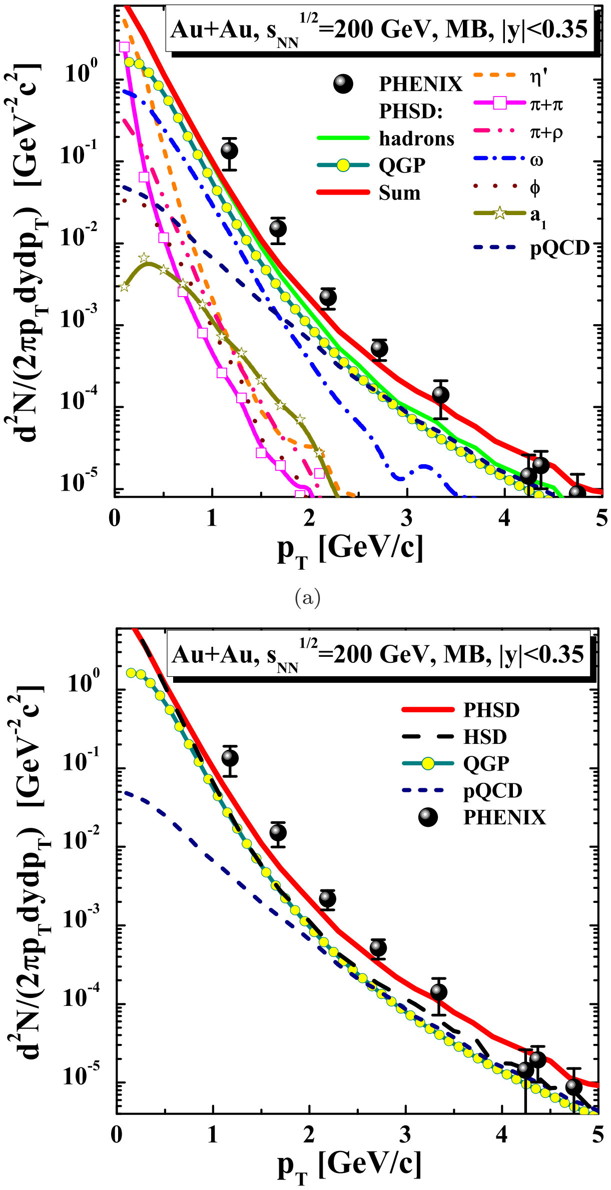

(a)

(b)

FIG. 3: (Color on-line) Top panel: Direct photons (all channels except the π- and η-meson decays) from the PHSD approach (red solid line) in comparison to the data of the PHENIX Collaboration [36, 37] for minimal bias collisions of Au+Au at $\sqrt{s_{NN}} = 200$ GeV (black symbols). The various channels are described in the legend. Bottom panel: Direct photon yield form PHSD (solid line) and hadron/string model HSD (dashed line) in comparison to the data of PHENIX Collaboration and the hard pQCD contribution (short-dashed line).

is significantly higher than for the photons emitted by mesons and their interactions after hadronization.

However, the 'effective temperature' discussed above is just the slope parameter of the transverse momentum spectrum and does not directly represent the temperature of the medium in which the photons are produced.

γ(QGP)	γ(hadronic)	PHSD Sum	PHENIX [37]
260 ± 10	170 ± 10	220 ± 10	233 ± 14 ± 19

TABLE I: Slope parameter T_{eff} (in MeV) of the direct photon spectrum for minimal bias Au+Au collisions at $\sqrt{s_{NN}} = 200$ GeV.

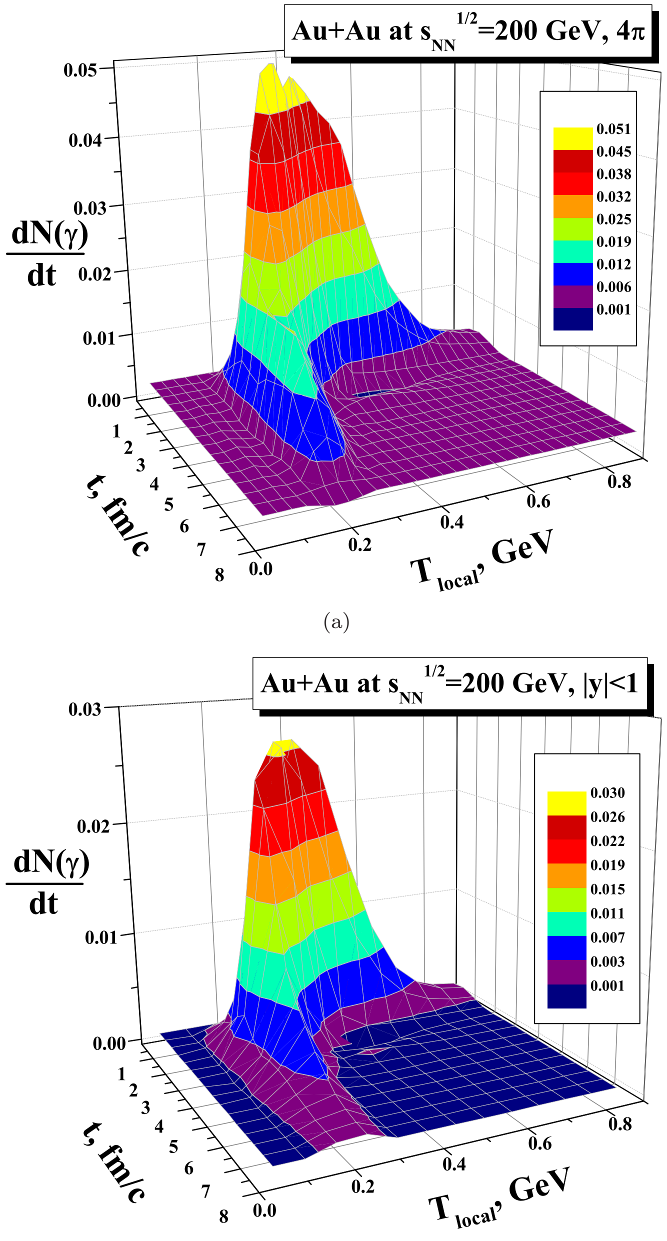

(a)

(b)

FIG. 4: (Color on-line) The photon production rate versus time and the local 'temperature' at the production point in (a) 4π and (b) mid-rapidity Au+Au collisions.

We recall that PHSD does not assume global or local thermal equilibrium, since the produced matter, at least initially, is far from equilibrium. Consequently, at each time step, the photons are produced in an ensemble of microscopic cells with different local energy density, which varies considerably from cell to cell. We can study the distribution in the local energy density of photon production in relativistic heavy-ion collisions as a function of time. The results are presented in Fig. 4, where for illustration purposes the energy density scale was recalculated into a temperature scale using the lattice QCD equation of state in equilibrium from Ref. [51]. Fig. 4 shows the photon production rate in the QGP as created in heavy ion collisions at $\sqrt{s_{NN}} = 200$ GeV versus time and the local 'temperature'. It is clearly seen that no universal 'temperature' can be assigned to the whole volume of the QGP (even in the mid-rapidity region). Instead we see a broad distribution of 'temperatures', which becomes narrower with time (partial equilibration) with the average temperature gradually decreasing (cooling). The temperature varies less, if mid-rapidity cut is applied. But even in this case ($|y| < 1$) the produced QGP does not fully reach equilibrium in the first 5 fm/c, which dominate the direct photon production.

B. Elliptic flow

Since about 50% of the direct photons measured by PHENIX stem from the collisions of quarks and gluons in the deconfined medium created in the initial phase of the collision, we first investigate the amount of elliptic flow that is carried by the colliding ('parent') partons. Note that the cross sections of the $q + \bar{q} \to g + \gamma$ and $q + g \to q + \gamma$ processes are isotropic in the azimuthal angle, thus the azimuthal asymmetry of the produced photons is generated from the direction of the summed initial momenta of the colliding partons ($\vec{p}_1, \vec{p}_2$), i.e. $\vec{q} = \vec{p}_1 + \vec{p}_2$. In Fig. 5 we show (top panel) the asymmetry $(q_X^2 - q_Y^2)/(q_X^2 + q_Y^2)$ for the total momentum $\vec{q}$ of the quark+antiquark (quark+gluon) pairs, which have suffered a collision and produce a photon through the $q + \bar{q} \to g + \gamma$ ($q + g \to q + \gamma$) process. The bottom panel of the Fig. 5 presents the number of such collisions versus time. We observe that the parton collisions - producing photons - take place throughout the evolution of the collision but the collision rate falls rapidly with time and thus the production of photons from the QGP is dominated by the early times. As a consequence, the elliptic flow 'picked up' by the photons from the parent parton collisions (given by the black solid line in the top panel of Fig. 5) saturates after about 5 fm/c and reaches a relatively low value of about 0.02, only. In comparison to the elliptic flow of the finally produced hadrons, the v_2 of the QGP photons is lower by an order of magnitude.

In Fig. 6 we show the v_2 of pions as calculated in the PHSD transport approach in comparison to the data from the PHENIX and STAR Collaborations [2, 52, 53]. One can see that the v_2 of produced π-mesons reaches $v_2 \approx 0.15$ and is well reproduced by the PHSD calculations as a function of the meson transverse momentum p_T. Note that in all the calculations presented in Figs. 6,7,8 the reaction plane correction has been applied event-by-event. The strong elliptic flow of hadrons for momenta $p_T < 3$ GeV - dominantly produced in the hadronization process - has the following origin: The dynamical hadronization happens at the end of the QGP evolution, i.e. when the elliptic flow of partons has already developed. Thus the hadrons pick up the collective acceleration of the partons. Contrary, photons from partonic interactions are essentially radiated during the first few fm/c of the collision dynamics in the central area of high energy density, while no mesons are produced in this space-time regime. We recall that the PHSD successfully describes of the total v_2 of final hadrons, while the purely hadronic scenario (HSD) leads to a substantial underes-

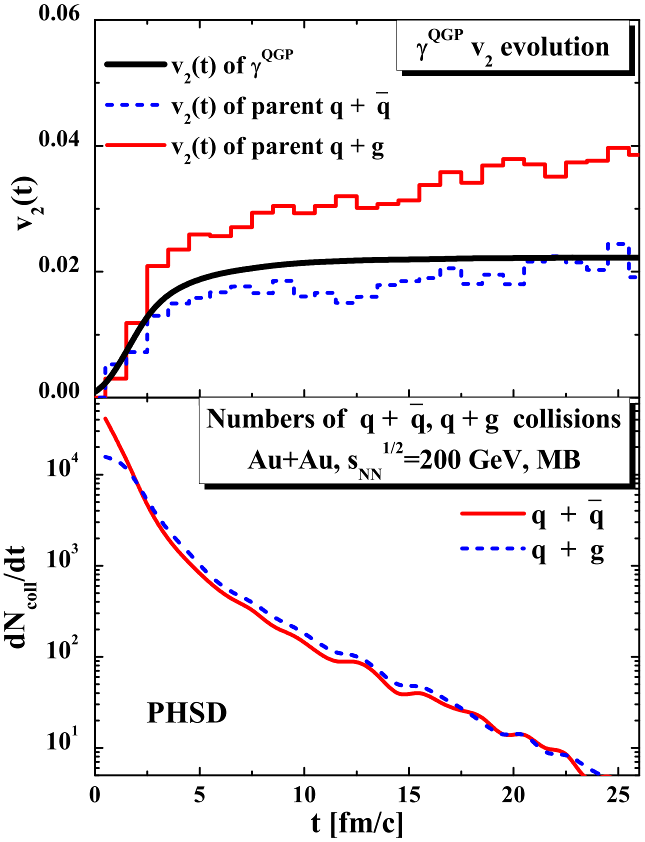

FIG. 5: (Color on-line) The azimuthal asymmetry of the momentum distribution for the parent partons - producing photons - and the time evolution for the elliptic flow v_2 of the photons created in these collisions (top panel). The number of photon-producing collisions as a function of time (bottom panel) for minimal bias Au+Au collisions at $\sqrt{s_{NN}} = 200$ GeV.

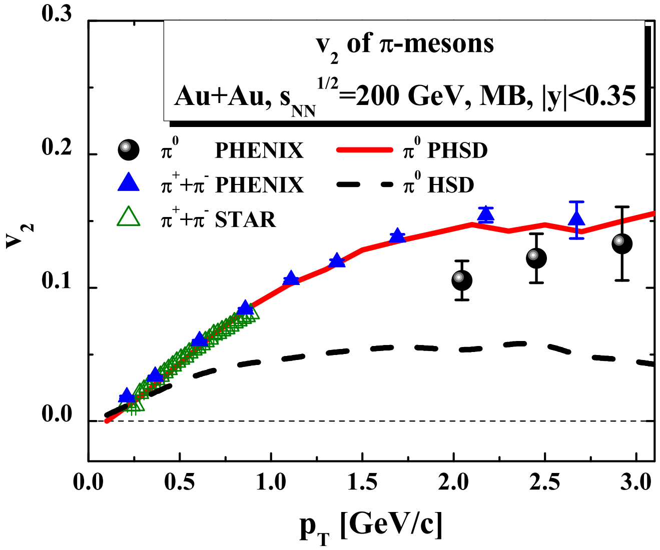

FIG. 6: (Color on-line) Elliptic flow of neutral pions from the PHSD approach (red solid line) and the data for the neutral and charged pion v_2 [2, 52, 53] for minimal bias Au+Au collisions at $\sqrt{s_{NN}} = 200$ GeV. The result from HSD is displayed by the dashed line.

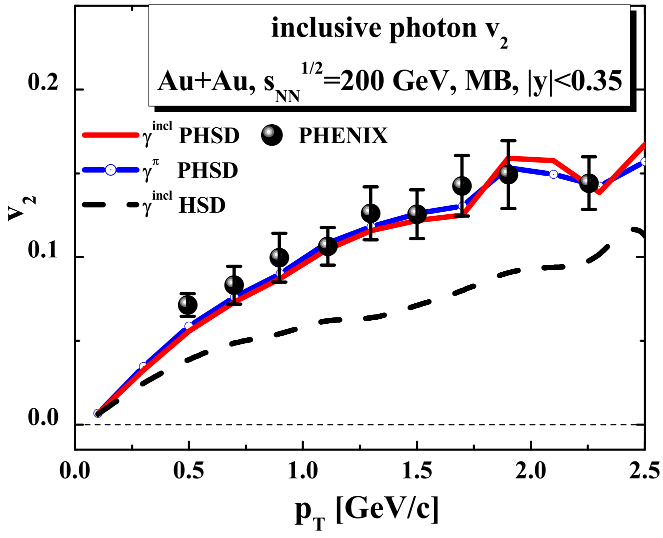

FIG. 7: (Color on-line) Elliptic flow of inclusive photons from the PHSD approach for minimal bias Au+Au collisions at $\sqrt{s_{NN}} = 200$ GeV. The data are from Ref. [2]. The result from HSD is displayed by the dashed line.

timation of elliptic flow [54], manly due to the lack of partonic interactions and a repulsive parton mean-field potential. We confirm this conclusion by presenting the p_T-dependence of the pion elliptic flow from the HSD approach in Fig. 6 for comparison (dashed line).

Next, we present in Fig. 7 the elliptic flow of the inclusive photons produced in minimal bias Au+Au collisions at $\sqrt{s_{NN}} = 200$ GeV from the PHSD (red solid line) and the experiment as measured by the PHENIX Collaboration. Please note that the PHSD calculations have about 10-15% statistical uncertainty which is not shown explicitly in the plot. We find that the data are reproduced within errors. The blue line with symbols shows the calculated v_2 of photons produced in pion decays. As we have seen above, the pion decay photons dominate the inclusive photon spectrum. Since the elliptic flow of pions is under control in PHSD (cf. Fig 6), the total photon v_2 is naturally also well described. Again, the HSD line calculated in the absence of the QGP (dashed line) underestimates the data by about a factor of 2.

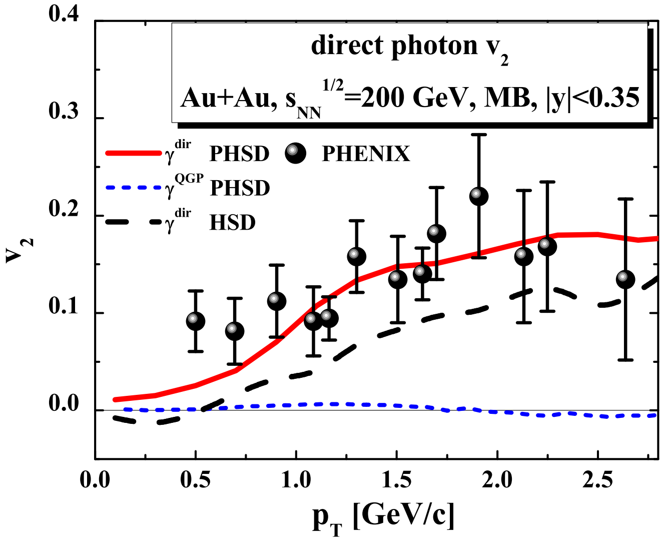

FIG. 8: (Color on-line) Elliptic flow of direct photons (π^0 and η decays excluded) in line with Eq. (6) from the PHSD approach for minimal bias Au+Au collisions at $\sqrt{s_{NN}} = 200$ GeV. The data are from Ref. [2]. The result from HSD is displayed by the dashed line.

The elliptic flow of direct photons $v_2(\gamma^{dir})$ is shown in Fig. 8. On the experimental side, this quantity was extracted from the measured inclusive photon $v_2(\gamma^{incl})$ by the substraction of the dominant hadron sources (π and η decays) as follows [2]:

$$v_2(\gamma^{dir}) = \frac{v_2(\gamma^{incl})N(\gamma^{incl}) - v_2(\gamma^{\pi})\left(N(\gamma^{\pi}) + N(\gamma^{\eta})\right)}{N(\gamma^{incl}) - N(\gamma^{\pi}) - N(\gamma^{\eta})} \quad (9)$$

where $N(\gamma^{incl})$ denotes the total measured photon yield, $(N(\gamma^{\pi}) + N(\gamma^{\eta}))$ is the yield of photons produced in the decays of π and η mesons, $v_2(\gamma^{\pi})$ the elliptic flow of photons stemming from π^0-meson decays. Note that equation (9) implies the approximation $v_2(\gamma^{\eta}) \approx v_2(\gamma^{\pi})$. We have followed the same procedure in the PHSD calculations which leads to the red solid line in Fig. 8. Please note that, as in the above plot, there is a statistical uncertainty in the PHSD results of about 10-15%.

The data on the direct photon v_2 are described also by the PHSD calculations such that we find no evidence for 'new physics'. On the other hand, the large v_2 of direct photons is a signal of the QGP produced in the early stages of the collision. The strong interaction in the partonic medium is a necessary prerequisite for the effective transfer of the collision eccentricity into the asymmetry of the hadron momentum distribution in the late stages, which in turn reflects in the v_2 of the produced photons. Indeed, the direct photon v_2 is underestimated in the purely hadronic scenario (dashed line in Fig. 8).

IV. CONCLUSIONS

In this study we have calculated the momentum spectra and the elliptic flow v_2 of photons produced in minimal bias Au+Au collisions at $\sqrt{s_{NN}} = 200$ GeV using the microscopic PHSD transport approach. For photon production we have incorporated the interactions of quarks and gluons in the strongly interacting quark-gluon plasma (sQGP) ($q + \bar{q} \to g + \gamma$ and $q(\bar{q}) + g \to q(\bar{q}) + \gamma$), the photon production in the hadronic decays ($\pi \to \gamma+\gamma$, $\eta \to \gamma+\gamma$, $\omega \to \pi+\gamma$, $\eta' \to \rho+\gamma$, $\phi \to \eta+\gamma$, $a_1 \to \pi+\gamma$) as well as the hadronic interactions ($\pi + \pi \to \rho + \gamma$, $\rho+\pi \to \pi+\gamma$) of intermediate mesons produced throughout the evolution of the collision. We have calculated the photon production in the elementary off-shell quark and gluon interactions by evaluating the tree-level diagrams for the photon production in the scattering of massive, broad quarks and gluons. The mesonic channels are treated as in the earlier Hadron-String Dynamics (HSD) analysis of photon production at lower collision energies [19].

We find that the PHSD calculations reproduce the transverse momentum spectrum of direct photons as measured by the PHENIX Collaboration in Refs. [36, 37]. We note, additionally, that the electric conductivity of the QGP from PHSD, which controls the photon emission rate in equilibrium, is rather well in line with available lQCD results [55]. Our microscopic calculations access the channel decomposition of the observed direct photon spectrum and show that the photons produced in the QGP constitute the largest contribution (about 50%) with the rest being distributed among the other channels: mesonic interactions, decays of massive hadronic resonances and the initial hard scatterings.

We, furthermore, have demonstrated that the elliptic flow of pions and the inclusive photon v_2 from PHSD are in a reasonable agreement with the PHENIX data for the same observables. When applying the same substraction procedure for the 'direct photon elliptic flow' as the PHENIX Collaboration (6) we find a rather good description of the photon v_2. Our calculations show that the photon production in the QGP is dominated by the early phase (similar to hydrodynamical models) and is localized in the center of the fireball, where the collective flow is still rather low, i.e. on the 2-3 % level, only. Thus, the strong v_2 of direct photons - which is comparable to the hadronic v_2 - in PHSD is attributed to hadronic channels, i.e. to the meson binary reactions and the resonance decays, which are not subtracted in the data. On the other hand, the strong v_2 of the 'parent' hadrons, in turn, stems from the interactions in the QGP via collisions and the partonic mean-filed potentials. Accordingly, the presence of the QGP shows up 'indirectly' in the direct photon elliptic flow.

Finally, the high 'effective temperature' of the direct photons is a strong evidence for the photon emission from the QGP. The experimental value of $T_{eff}(\text{exp}) = 233 \pm 19$ MeV can not be explained by the photons of hadronic origin, even though the "blue shift" due to the radial collective motion leads to a slope parameter $T_{eff}(\text{hadrons}) = 170 \pm 10$ MeV, which is above the critical temperature in our model $T_C = 158$ MeV. On the other hand, the partonic contribution to the photon spectrum has a considerably higher $T_{eff}(\text{QGP}) = 260 \pm 10$ MeV. Taking into account both the partonic and hadronic sources of photons, we obtain within PHSD $T_{eff}(\text{PHSD}) = 220 \pm 10$ MeV and, therefore, reproduce the measured 'effective temperature'. Our findings imply that there is presently no clear signal for 'unconventional physics' (beyond the strong interaction on the partonic and hadronic level) in the photon data from the PHENIX Collaboration.

Acknowledgements

The authors are grateful for fruitful discussions with A. Drees, C. Gale, H. van Hees, C.M. Ko, V. Koch, L. McLerran, R. Petti, R. Rapp, V. Skokov, E. Shuryak, R. Venugopalan and N. Xu. This study was supported by the LOEWE center HIC for FAIR and the Margarete-Bieber Program at the University of Giessen.

---

[1] T. Peitzmann and M. H. Thoma, Phys.Rept. **364**, 175 (2002).
[2] A. Adare et al. (PHENIX Collaboration), Phys.Rev.Lett. **109**, 122302 (2012).
[3] R. Chatterjee, E. S. Frodermann, U. W. Heinz, and D. K. Srivastava, Phys.Rev.Lett. **96**, 202302 (2006).
[4] F.-M. Liu, T. Hirano, K. Werner, and Y. Zhu, Nucl.Phys. **A830**, 587C (2009).
[5] M. Dion, C. Gale, S. Jeon, J.-F. Paquet, B. Schenke, et al., J.Phys. **G38**, 124138 (2011).
[6] M. Dion, J.-F. Paquet, B. Schenke, C. Young, S. Jeon, et al., Phys.Rev. **C84**, 064901 (2011).
[7] A. Bzdak and V. Skokov (2012), 1208.5502.
[8] G. Basar, D. Kharzeev, D. Kharzeev, and V. Skokov, Phys.Rev.Lett. **109**, 202303 (2012).
[9] V. Goloviznin, A. Snigirev, and G. Zinovjev (2012), 1209.2380.
[10] V. Pantuev (2011), 1105.4033.

[11] H. van Hees, C. Gale, and R. Rapp, Phys. Rev. **C84**, 054906 (2011).

[12] E. Bratkovskaya, W. Cassing, V. Konchakovski, and O. Linnyk, Nucl.Phys. **A856**, 162 (2011).

[13] O. Linnyk, E. L. Bratkovskaya, V. Ozvenchuk, W. Cassing, and C. M. Ko, Phys.Rev. **C84**, 054917 (2011).

[14] O. Linnyk, W. Cassing, J. Manninen, E. Bratkovskaya, and C. Ko, Phys.Rev. **C85**, 024910 (2012).

[15] O. Linnyk, W. Cassing, J. Manninen, E. Bratkovskaya, P. Gossiaux, et al., Phys.Rev. **C87**, 014905 (2013).

[16] W. Cassing and E. L. Bratkovskaya, Phys. Rept. **308**, 65 (1999).

[17] E. L. Bratkovskaya and W. Cassing, Nucl. Phys. **A 619**, 413 (1997).

[18] W. Ehehalt and W. Cassing, Nucl. Phys. **A 602**, 449 (1996).

[19] E. Bratkovskaya, S. Kiselev, and G. Sharkov, Phys.Rev. **C78**, 034905 (2008).

[20] J. Adams et al. (STAR Collaboration), Nucl.Phys. **A757**, 102 (2005).

[21] K. Adcox et al. (PHENIX Collaboration), Nucl.Phys. **A757**, 184 (2005).

[22] I. Arsene et al. (BRAHMS Collaboration), Nucl.Phys. **A757**, 1 (2005).

[23] B. Back, M. Baker, M. Ballintijn, D. Barton, B. Becker, et al., Nucl.Phys. **A757**, 28 (2005).

[24] E. L. Bratkovskaya, W. Cassing, V. P. Konchakovski, and O. Linnyk, Nucl. Phys. **A856**, 162 (2011).

[25] E. L. Feinberg, Nuovo Cim. **A34**, 391 (1976).

[26] E. V. Shuryak, Phys. Lett. **B78**, 150 (1978), Sov. J. Nucl. Phys. **28** 408 (1978), Yad. Fiz. **28** 796 (1978).

[27] J. I. Kapusta, P. Lichard, and D. Seibert, Phys.Rev. **D44**, 2774 (1991).

[28] J.-e. Alam, S. Sarkar, T. Hatsuda, T. K. Nayak, and B. Sinha, Phys.Rev. **C63**, 021901 (2001).

[29] F. D. Steffen and M. H. Thoma, Phys.Lett. **B510**, 98 (2001).

[30] D. K. Srivastava and B. Sinha, Phys.Rev. **C64**, 034902 (2001).

[31] P. Huovinen, P. Ruuskanen, and S. Rasanen, Phys.Lett. **B535**, 109 (2002).

[32] S. Turbide, R. Rapp, and C. Gale, Phys.Rev. **C69**, 014903 (2004).

[33] D. G. d'Enterria and D. Peressounko, Eur.Phys.J. **C46**, 451 (2006).

[34] F.-M. Liu, T. Hirano, K. Werner, and Y. Zhu, Phys.Rev. **C79**, 014905 (2009).

[35] S. Turbide, C. Gale, E. Frodermann, and U. Heinz, Phys.Rev. **C77**, 024909 (2008).

[36] A. Adare et al. (PHENIX), Phys. Rev. **C 81**, 034911 (2010).

[37] A. Adare et al. (PHENIX Collaboration), Phys.Rev.Lett. **104**, 132301 (2010).

[38] E. L. Bratkovskaya, W. Cassing, and O. Linnyk, Phys. Lett. **B670**, 428 (2009).

[39] W. Cassing and E. L. Bratkovskaya, Nucl. Phys. **A 831**, 215 (2009).

[40] W. Cassing and E. L. Bratkovskaya, Phys. Rev. **C 78**, 034919 (2008).

[41] W. Cassing and S. Juchem, Nucl. Phys. **A 665**, 377 (2000), *ibid.* A **672**, 417 (2000).

[42] W. Cassing, Eur. Phys. J. ST **168**, 3 (2009).

[43] O. Linnyk, E. Bratkovskaya, J. Manninen, and W. Cassing, J.Phys.Conf.Ser. **312**, 012010 (2011).

[44] J. Beringer et al. (Particle Data Group), Phys.Rev. **D86**, 010001 (2012).

[45] C. Song, C. M. Ko, and C. Gale, Phys. Rev. **D50**, 1827 (1994).

[46] C. Song, Phys.Rev. **C47**, 2861 (1993).

[47] S. Marzani and R. D. Ball, Nucl.Phys. **B814**, 246 (2009).

[48] C.-Y. Wong and H. Wang, Phys.Rev. **C58**, 376 (1998).

[49] O. Linnyk, S. Leupold, and U. Mosel, Phys. Rev. **D71**, 034009 (2005).

[50] O. Linnyk, J. Phys. **G38**, 025105 (2011).

[51] S. Borsanyi et al. (Wuppertal-Budapest Collaboration), JHEP **1009**, 073 (2010).

[52] J. Adams et al. (STAR Collaboration), Phys.Rev. **C72**, 014904 (2005).

[53] S. Adler et al. (PHENIX Collaboration), Phys.Rev.Lett. **91**, 182301 (2003).

[54] V. Konchakovski, E. Bratkovskaya, W. Cassing, V. Toneev, S. Voloshin, et al., Phys.Rev. **C85**, 044922 (2012).

[55] W. Cassing, O. Linnyk, T. Steinert, and V. Ozvenchuk (2013), Phys. Rev. Lett., in press, arXiv:1302.0906.